Chapter 6
Catalytic Efficiency in Metallic Nanoparticles: A Computational Approach

Hector Barron

6.1 Introduction

Computational modelling and simulations are among the most significant developments in the practice of scientific inquiry in the twentieth century. Within the past few decades, scientific computing has become an important contributor to all scientific research programmes. It is particularly important for the solution of research problems that are insoluble by traditional theoretical and experimental approaches, hazardous to study in the laboratory or time-consuming or expensive to solve by common techniques. Under this context, computational simulations have change from merely performing a calculation to become *virtual* laboratories in which a system can be studied from a different perspective. This triggered the rise of a wide variety of modelling techniques developed over the years, including the models to study systems at the molecular level such as molecular dynamics (MD), classical Monte Carlo [1, 2], quantum-based techniques [3] and Monte Carlo methods [4], and MD combined with electron density functional theory. The results of model simulations help researchers make predictions about what will happen in the real system that is being studied in response to changing conditions. Modelling can expedite research by allowing scientists to conduct thousands of simulated experiments by computer in order to identify the actual physical experiments that are most likely to help the researcher find the solution to the problem being studied.

Over the past decade, computational methods in catalysis have attracted a widespread interest as means for investigating the underlying pathways of an overall reaction and providing insights into the design of suitable catalysts [5–8]. As in many other areas of materials science, modern computational science is

H. Barron (✉)
CSIRO, Molecular and Materials Modelling, Data61, Door 34 Goods Shed Village St, 3008, Docklands, VIC, Australia
e-mail: hector.barronescobar@data61.csiro.au

becoming a key contributor in the quest to quantitatively understand the molecular-level mechanisms underlying the macroscopic phenomena in chemical processing, envisioned to ultimately enable a rational design of novel catalysts and improved production strategies.

Of particular relevance are hierarchical approaches that link the insights that modelling and simulation can provide across all relevant length and time scales. For example, first-principles methods, such as the widely used density functional theory (DFT), can be employed at the molecular scale to understand the elementary events and the reaction mechanisms giving rise to catalytic activity. Application of DFT methods can be found in studies of the stability of Ni catalysts for steam reforming by the addition of gold, the mixing of cobalt and molybdenum in ammonia synthesis catalysts [5], new mixed transition metal sulphides for hydrodesulphurisation [9], new CO-tolerant alloys for fuel-cell anodes [10] and near-surface alloys for hydrogen activation [11]. With the success of this approach, an extensive computational screening of surface structures for new catalysts was performed for the methanation reaction [12].

Another important theoretical approach to study the activity and selectivity at the catalyst scale is the kinetic models. Some of these models may employ Langmuir-Hinshelwood-type models [7], Sabatier analysis [13], mean-field micro-kinetic models or more sophisticated statistical-mechanical treatments, in particular kinetic Monte Carlo (KMC) simulation [14, 15]. The latter is motivated by the structural complexity exhibited by heterogeneous catalysts, which expose several different types of sites that may have distinct functionalities. For instance, sites at the interface between metal and support may behave differently than these two phases, planar versus low coordinated sites or defects may exhibit disparate catalytic activity, and alloys may expose a variety of sites at the interface of the two (or more) components. KMC models have indeed been successfully used to unravel such complexities and aid in catalyst discovery; recent studies on ethanol synthesis from syngas identified effective promoters for Rh-based catalysts and made connections with experiments [16, 17].

More recently, Barron et al. [18] studied the nucleation, growth and catalytic activity of Pt nanoparticles by using classical molecular dynamics (CMD). The structures obtained exhibit surfaces characterised by a high free energy and a much higher density of steps, kinks and terraces (composed of atoms with low coordination number) than ideal polyhedra, making them highly desirable for use in various types of catalytic reactions. By using a classification of those surface defects, it was possible to link each of those groups to a specific catalytic reaction.

In this perspective, we first review some of the computational techniques available to investigate some of the most important catalytic reactions from first principles to kinetic Monte Carlo to shed light on specific chemistries. Furthermore, we show how CMD simulations can be an alternative method to *ab initio* models in the design of novel nanocatalysts by tuning the nucleation and growth process obtaining particles with high density of surface defects. Finally, we propose directions for future research towards achieving these goals.

6.2 *Ab Initio* Calculations

Extensive theoretical and computational approaches have been employed to try to meet the goal of developing a fundamental understanding as a basis for catalyst design [6]. The solution of the Schrödinger equation to obtain the energy of a given configuration of nuclei and their electrons is a nontrivial task even for small systems, and it becomes especially arduous when the system involves multiple phases as is the case in a surface reaction. The formal cornerstone of DFT is a theorem derived by Hohenberg and Kohn [22], which states that the ground-state electronic energy is a unique functional of the electronic density $n(\mathbf{r})$, with $\mathbf{r}$ the space coordinate. In other words, there exists a one-to-one correspondence between the $\mathbf{r}$-dependent electronic density of the system and the energy. Further development of this method was conducted by Kohn and Sham in 1965 [23]. They decomposed the exact kinetic energy functional into two parts to approximate the universal functional. However, the exact functional giving the exact energy is not known, and in practice one must therefore resort to one of the many approximate expressions available. The quality of these functionals is now such that one may calculate overall energies to within an accuracy of about 5–10 % of the exact result, which is sufficient for many purposes. DFT calculations nevertheless provide useful and important perspectives on chemical reactions that are not accessible through experimental observations alone.

6.2.1 *Electrocatalysis*

The field of electrocatalysis has recently undergone a significant resurgence in research activity. This is due to several factors including the urgent need to create better technologies in a clean and sustainable manner [12, 14, 19, 24, 71]. The electrochemical processes always involve multiple reaction pathways, active sites and products and cannot be well characterised experimentally. The development of DFT in electrochemistry makes it possible to understand the reaction mechanism at the atomic level. Such understanding allows the theoretical screening for better catalysts. In order to model electrochemical systems, several factors have to be modelled simultaneously: the structure and chemistry that occur at the anode and the cathode, the electron transfer between the two electrodes and the local changes in the electrolytes. To this end, various approximated approaches have been developed to simulate the electrochemistry, which describe the solid electrode surface, the liquid solution, the solvated ions and the effect of changes in the chemical potential of the electrons in the solid.

6.2.1.1 Description of Different Electrochemical Reactions

One of the most important advances in DFT is in the accurate description of electrocatalytic reactions at surfaces with great detail. The method developed by Neurock et al. [27] described qualitatively various electrochemical reactions, water activation, oxygen reduction reaction (ORR) as well as methanol decomposition on metal surfaces, being able to gain insights into the reaction mechanism under potential over aqueous-metal interfaces [26, 28, 29]. The ORR is a canonical chemical reaction due to its ubiquitous presence in corrosion, combustion, energy conversion and storage processes. Besides its importance in basic electrochemistry, the oxygen reduction reaction is also relevant to energy conversion in polymer electrolyte membrane fuel cells (PEM-FCs). In principle, gaseous H_2 is oxidised at the anode, and its protons migrate through the electrolyte to the cathode where they finally react with O_2 under uptake of four electrons to form two water molecules. Despite the apparently simple reaction mechanism and thus the fundamental reaction steps of the ORR are still not fully understood. Indeed, this reaction is highly complex since it occurs in a multicomponent environment and is influenced by various environmental parameters: temperature, pressure and electrode potential. Another method to describe the electrochemistry, which gives in some cases accuracy required for computational results to compare with experiment in a meaningful way, was proposed by Norskov [30]. In this work, DFT calculations and a micro-kinetic modelling are combined to describe the H_2/CO electro-oxidation on Pt and Pt alloy surfaces. The model is very simple and is able to express the kinetics of a promoted anode surface relative to the activity of pure Pt directly from the calculated adsorption energy differences. DFT-based studies also provide the understanding of changes in catalytic activity from one catalyst to another, which is also qualitatively comparable to the experimental measurement [30–34]. This allows more insight into the reaction mechanism. Both experiment and theory show that PtRu and Pt_3Sn are better electrocatalysts than Pt, being able to oxidise H_2 and CO at lower potential; in contrast, higher potential should be applied to oxide CO on Ru. Within the model, the origin of the promoting effect of alloying can be analysed. That is, the promoting effect of alloying on H_2/CO oxidation reaction can be attributed to the fact that alloyed metals modify Pt in the surface to bond CO weaker, thus decreasing the CO coverage under working conditions of the electrode. Such detailed understanding cannot be achieved merely using experimental techniques and is very important to the rational catalyst screening.

6.2.2 Future Directions

Even though some progress has been made towards understanding electrocatalytic process and screening electrocatalysts from DFT, the method has difficulty in providing quantitative numbers for detailed reaction steps. DFT studies are too

simplified to model the real catalysts effectively. For example, some fabricated catalysts are powders, which may behave differently with size. Recently, efforts have been made to model the nanoparticles with the size of experimental catalysts (5 nm), showing indeed different behaviours from the extended surfaces [35, 36]. Thus, theoretical predictions based on the calculations of extended surfaces may not necessarily be able to describe the electrocatalysts with small size. In addition, the electrochemical processes may always be complex, including multiple reaction pathways, rate-limiting steps and products. As a consequence, more sophisticated models are needed to capture knowledge for catalyst optimisation. With the further development of DFT method and models that can effectively treat more realistic catalysts and their environments, it can be envisioned that soon DFT modelling in electrochemistry will not only provide insight into the experimental measurements but also become the standard choice for designing a new catalyst for a catalytic process.

6.3 Monte Carlo

This method is especially useful for studying catalytic reactions taking place on the reaction sites of a catalyst surface. The evolution of the entire system is obtained by solving the so-called master equation (Eq. 6.1) using an MC-type algorithm [37–40].

$$\frac{dP_\alpha}{dt} = \sum_\beta [k_{\alpha\beta} P_\beta - k_{\beta\alpha} P_\alpha].$$
(6.1)

Equation 6.1 describes the evolution of probability P_α for the system being in the surface configuration state α. Here, $k_{\alpha\beta}$ defines the transition probability from state α to state β. The transition in the sense of surface simulation can, for instance, be a diffusion step or a reaction with rate $k_{\alpha\beta}$. Analytical solutions to the master equation can be derived only for simple cases. In general, a numerical solution is required. A MC simulation starts from a state α and repeatedly picks a random possible process and advances in time. Averaging over several trajectories leads to a numerical solution of the master equation. This algorithm is designed such that the exact time dependence is obtained, i.e. that the subsequent configurations generated satisfy the correct detailed balance. Kinetic Monte Carlo (KMC) is the method of choice for the micro-kinetic modelling of catalytic reactions on surfaces when ordering, island formation and slow surface mobility are of our interest. Although kinetics plays such an important role in catalysis, its theory has for a long time mainly been restricted to the use of macroscopic deterministic rate equations. These implicitly assume a random distribution of adsorbates on the catalyst surface. Effects of lateral interactions, reactant segregation, site blocking and defects have only been described *ad hoc*.

6.3.1   KMC Approach in Catalysis

KMC methods have been used to simulate the catalytic surface chemistry for various different reaction systems. The vapour-phase oxidation of CO to form CO_2, however, has been the most widely studied due to its simplicity as well as its general applicability. Pioneering work by Ziff [41] and Neurock [14] shows the formations of interesting phase transitions as a function of the kinetics and lateral interactions. Many subsequent studies by various other groups extend the basic models to cover more general features.

6.3.1.1   CO Oxidation

The CO oxidation chemistry has attracted significant attention over the past decade, since its simplicity enables detailed modelling. This chemistry is of environmental importance for removing toxic CO from exhausts [15]. The CO oxidation on RuO_2 (110) has been extensively investigated by Reuter, Scheffler and co-workers [15, 42, 44–47]. In those studies, the RuO_2(110) surface was modelled as a lattice with two types of sites, bridge and cus. The adsorption of O_2 (dissociative) and CO, the diffusion of adsorbed CO and atomic oxygen as well as the CO_2 formation were analysed with DFT, and the parameters were incorporated into a first-principles MC framework. The simulation results were in agreement with experimental data for conditions ranging from ultrahigh vacuum (UHV) to industrially relevant pressures [15, 43]. The CO oxidation reaction has also been modelled on metal catalysts, in particular Pt, Rh and Pd single crystal surfaces and Au nanoclusters [51]. Volkening and Wintterlin [50] presented KMC simulations of this reaction on Pt (111). This model was subsequently extended to incorporate coordination-dependent reactivity, thereby being able to reproduce experimental observations, in particular, the reaction order of 1/2 with respect to oxygen coverage, the shapes of the domains occupied by adsorbed CO and O, as well as the higher reactivity of the domain boundaries. Furthermore, Rogal et al. [48] studied the CO oxidation chemistry on Pd (100) and showed that a surface oxide structure can be stable at ambient pressures, under which the surface can be catalytically active. They postulated that at steady state, transitions between the reduced and the oxidic Pd (100) structure may take place. In a detailed study, Liu and Evans [49] used KMC simulation in a multiscale modelling context, to simulate the CO oxidation on Rh (100) and Pd (100). The simulations were found to be in good agreement with experimentally obtained TPR spectra and provided insight into the onset of propagating reaction fronts at mesoscale. Finally, Stamatakis et al. [51] recently investigated the reaction rates and poisoning effects for the CO chemistry on MgO supported Au6 nanoclusters.

6.3.1.2 NO Reduction and Oxidation

NO-related catalysis have also served as prototypes for the assessment of KMC modelling techniques and are of practical significance because of environmental and health impacts. Thus, several studies have investigated such chemistries using KMC models focusing on the impact of geometry for clusters of sites catalysing the NO reduction by CO [52–54], the effect of impurities blocking catalytic sites [53] as well as the effect of step sites [55] in this system, the adsorbate-induced phase transition and the oscillatory characteristics of NO reduction by NH_3 [56], as well as the different pathways and the effect of lateral interactions of NO decomposition during TPR experiments [57, 58]. Further, kinetic oscillations, reaction fronts and pattern formation phenomena for the NO chemistries have received much attention and have been simulated with deterministic models [59, 60] as well as KMC methods [61–67].

6.3.1.3 Ethylene Hydrogenation

The hydrogenation of ethylene is a prototype system of hydrogenation reactions and is important in the conversion of olefins into higher-octane gasoline blending components. An early KMC study of this reaction on Pt focused on diffusion, activation of surface intermediates and steric hindrance effects [68]. Hansen and Neurock developed a first-principles KMC model of ethylene hydrogenation on Pd (100), which utilised DFT calculated energetics at the zero coverage limit, whereas adsorbate lateral interaction effects were incorporated within the BOC framework [69]. Their model predicts an apparent reaction order which is negative with respect to ethylene and less than unity with respect to hydrogen, in agreement with experimental data. This work was later extended by Neurock and co-workers [14], to study Pd (111) as well as bimetallic Pd/Au (111) surfaces. It was found that higher surface Au compositions result in a strengthening of the metal-hydrogen and metal-carbon bonds, thereby promoting the hydrogenation activity, but also in a weaker binding of H_2 on the surface, which hinders the catalytic activity. Compensation between these two effects leads to alloying Au with Pd having an overall negligible effect of on the activity, consistent with experiments [70, 71]. Clearly, first-principles KMC constitutes a powerful and versatile multiscale modelling framework that can offer valuable insight into catalytic phenomena. Nevertheless, there are still major challenges in the development of accurate KMC methods with predictive power. These challenges may pertain to the inadequate description of the underlying physics and chemistry, as well as to the computational cost arising from the inefficiency of the simulation.

6.3.2   KMC Simulations for Catalysis in Nanoparticles

The study of catalytic reactions requires to model catalytic surfaces that are not uniform; site heterogeneity exists because the surface of practical catalyst particles is characterised by terraces of different crystal structures, steps, edges, additives, impurities and defects. Therefore, it is required to enable KMC simulations for such systems in order to derive technical meaningful rates and give insight into geometric and communication effects. Prior attempts have been made to perform KMC simulations on nanoparticles. One approach is to regard a single lattice without periodic boundary conditions as particle and describe the facets as different regions [72–74]. Another simulation approach uses three-dimensional particles, which can vary their height to mimic shape transformation. These models use a single lattice with additional information about the particle height for each adsorption place [75]. Both models neglect the nature of different facets regarding their neighbourhood because they are limited to one lattice type and cannot represent the different neighbourhoods of combinations like fcc(111) and fcc(100) faces. A hybrid approach between a lattice and an off-lattice method can overcome these limitations. The facets of the catalyst particle and the support are each described by a lattice, which are linked along their edges. Since such models lead to a high number of different processes, it is favourable to have a general implementation, which is not restricted to a specific mechanism and allows different particle shapes.

6.3.3   Future Directions

The impact of KMC simulation will mainly be manifested in problems incorporating spatial effects where multiple active sites are involved and the activity and selectivity arise from nonlinear coupling among these sites. Examples include the dependence of the structure sensitivity of a reaction on nanoparticle size and shape, promoters, whose specific location may be important, multifunctional materials (e.g. Lewis and Brønsted acid sites or metal and Brønsted acid sites) and support effects due to parts of the chemistry occurring on the support, the metal sites and interfacial support/metal sites. The ongoing efforts to incorporate more detailed physics and chemistry in these simulations in conjunction with the never-ending pursuit of more efficient methodologies is bound to improve the predictive power of first-principles KMC, making it a quantitative tool for mechanism understanding and eventually *in silico* catalyst discovery and optimisation.

6.4   Molecular Dynamics

In classical molecular dynamic methods [20], the atoms and molecules in the system of interest interact through many-body effective potentials. In this context, the word classical means that the nuclear motion of the constituent particles obeys the laws

of *classical* mechanics. The electronic and quantum nature of the system is not explicitly taken into account, and the time evolution of the system is obtained by solving Newton's classical equations of motion. Averaging of the CMD trajectories over a sufficiently long simulation period allows one to extract thermodynamic, dynamical and other macroscopic properties. If we consider a classical system Δ consisting of N particles, its microscopic state is described in terms of the positions $\mathbf{r}$ and momentum $\mathbf{p}$ of each particle. If V is the interparticle potential, then $V = V(\mathbf{r}_1, \ldots \mathbf{r}_N)$ and T the kinetic energy of the system; thus the Hamiltonian $H = T + V$ represents the total energy in the system. In a classical environment, being $\mathbf{r}_i$ the Cartesian coordinates, the time evolution of the system is given by the Newton equations:

$$m_i \ddot{\mathbf{r}} = \mathbf{f}_i \qquad (6.2)$$

where m_i is the mass of particles i and $\mathbf{f}_i = -\nabla \mathbf{r}_i H = -\nabla \mathbf{r}_i V$ is the force on particles i.

   CMD is one of the best tools to study nanocluster growth since it is possible to simulate, with the present computational resources, time scales comparable with the experimental ones. Moreover, by CMD it is not necessary to make any *a-priori* assumptions, as happens in KMC simulations [21, 22]. It's important to mention that molecular dynamics can be also be performed using ab *initio* methods that take into consideration the electronic nature of the system to calculate different properties [25].

6.4.1   Metallic Nanoparticles for Catalytic Applications

There has been a great interest in using nanocrystals as catalysts due to their high surface area-to-volume ratios and high surface energies, which make their surface atoms to be highly active [76]. Generally, catalytic performance of nanocrystals can be finely tuned not only by their composition, which mediates electronic structure, but also by their shape, which determines surface atomic arrangement and surface coordination [77]. In this context, metal nanoparticles exhibit a wide variety of shapes, facets and fraction of surface atoms, which makes it critically important to study the effect of metal nanoparticles shape on the catalytic activity of various organic and inorganic reactions. The shape sensitivity of nanocatalysts is attributed to electronic and geometrical effects that influence adsorption energies and reaction pathways [31]. The chemisorption of reaction species can occur preferentially on surface atoms with low coordination number allowing more energetically favourable transition states compared to close-packed surfaces [78–81]. The purpose of targeting specific shapes is to enrich samples with the greater density of specific types of under-coordinated atoms at the surface, with preference given to those with as lower atomic coordination number as possible. Each crystallographic facet has a characteristic surface atomic arrangement and degree of "under-coordination", and although this ultimately determines the concentration of active sites available

Fig. 6.1 Snap shot of the final stage from the formation of Pt nanoparticles. The main nuclei surrounded by small clusters as a consequence of coalescence and sintering can be seen as well as islands, kinks and steps decorating the cluster surface. In general, coalescence and sintering is more common to appear in cluster formed at slower deposition rates leading the formation of longer branches in their final stage
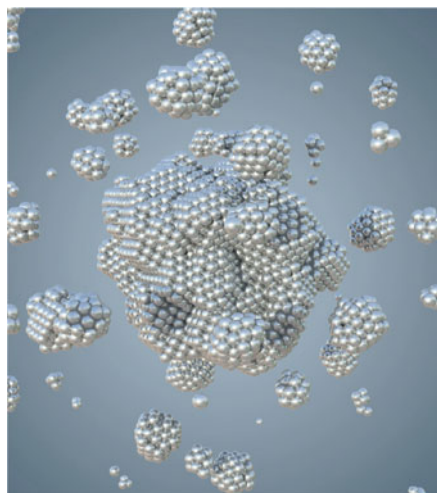
for reactions, it is still challenging to predict the structure-dependent activity *a-priori*. The structure-dependent activity can be empirically obtained; however the type of defect and performance in the nanocrystal is highly dependent in the polydispersivity of the sample, making this a challenging task. Alternatively, analytical models can be used to address the issue of sample diversity but in most predicative models are usually idealised [82]; the imperfections and surface defects omitted for simplicity. Defects, including stacking faults, kinks, steps and terraces, routinely appear during crystal growth, and the inclusion of these features in predictive models can yield important insights [83] (Fig. 6.1).

6.4.2 Nucleation Process of Catalytic Nanoparticles

Experimentally, the shape control synthesis has been widely investigated in order to find better strategies to manipulate particle growth processes, and these processes are also well described by computer simulations. Typically two types of CMD simulations are used to model this process: the single atom (or monomers) insertion to coalescence, under a specified set of conditions (often referred to as coarsening) [84–86], and via the collision of two preexisting particles to form a single aggregate which then undergoes restructuring, again under specific conditions (often referred to as sintering) [87]. In order to generate anisotropic nanoparticles with a high density of surface defects for catalytic applications, we adopted the first computational approach (single atom insertion) to investigate the relationship between the formation temperature and the growth rate with the degree of disorder in Pt nanoparticles. In this way, we related the initial conditions of the formation process with some simple indicators of catalytic efficiency, by tracking the density of different types of under-coordinated surface atoms as a function of time. The
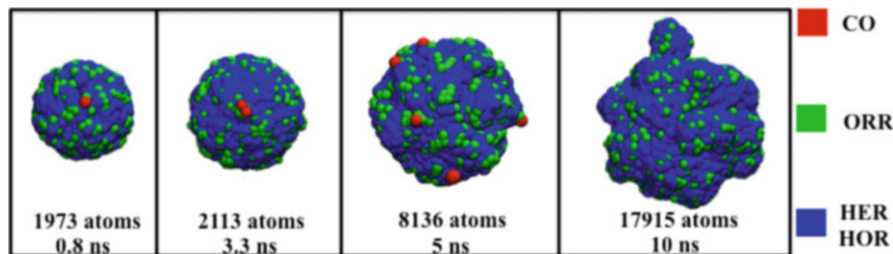
Fig. 6.2 Distribution of catalytically active sites in Pt nanoparticles. Atoms coloured in red (SCN of 1, 2 and 3) are active sites for carbon oxidation (CO) reactions, atoms in green (SCN of 4, 5, 6 and 7) are suitable for oxygen reduction reactions (ORR), and atoms in blue (SCN of 8, 9, 10 and 11) are suitable for hydrogen evolution reaction (HER) and hydrogen oxidation reactions (HOR)

CMD simulations were carried out using the LAMMPS code [88], under the embedded atom method (EAM), with a potential parameterised by Foiles et al. that proven to accurately describe the platinum atomic interactions [89]. The simulation consists in the random insertion of atoms at different temperatures of 30 °C, 100 °C and 200 °C, with atomic deposition rates (τ) of 1 atom each 5 simulation steps ($\tau = 2.5 \times 10^{-5}$ atoms per ns) and 1 atom each 100 simulation steps ($\tau = 5 \times 10^{-4}$ atoms per ns). The temperature values were chosen based on the experimental synthesis of Pt nanoparticles [90] and the deposition rates in accordance with previous computational studies [91]. The atoms were deposited for 2 and 5 ns depending on the atomic deposition rate (τ). The trajectories generated by the simulations were analysed to track the evolution of different types of surface defects, by quantifying the coordination numbers of all surface atoms (SCN) as a function of time (Fig. 6.2).

6.4.2.1 Classification of Surface Defects

During the nucleation process, nanoparticles experience different structural transformations due to the sintering, coalescence and the energetic competition between facets, giving rise to different surface defects. These defects can be classified according to their coordination number (SCN). In previous work we have established a simple classification scheme relating SCN to functional similarities [82]. For instance, all atoms with SCN of 1, 2 or 3 are classified as surface defects (adatoms placed on "top", "bridge" and "hollow" sites); atoms with SCN of 4, 5, 6 or 7 are termed surface microstructures (kinks/steps-like defects); and atoms with SCN of 8, 9, 10 or 11 are termed surface facets (surface-like defects that include any planar configuration). Each of these groups is linked to a specific catalytic reaction. For example, it has been well established that CO oxidation is initiated on step sites on (111) terraces and diffuses rapidly to surface defect sites [92, 93]. Surface microstructures are important in the first stage of CO reactions and oxygen reduction reactions (ORR) [92], since electrolyte anions adsorb more strongly on steps and

Fig. 6.3 Final morphologies obtained at the end of the simulations and their SCN distribution at different temperatures and atomic deposition rates (τ/atoms per ns). Lower coordinated atoms are localised on the tips and along the branches, while higher coordinated atoms occupy "flat" areas over the surface. Since atoms with SCN of 1, 2 and 3 are present at early stages during the simulation, the colour scale goes from SCN 4 (in grey) to SCN 11 (in red). Orange and red colours cover the majority of the surface; this means that SCN of 10 and 11 are dominant at the end of the simulation
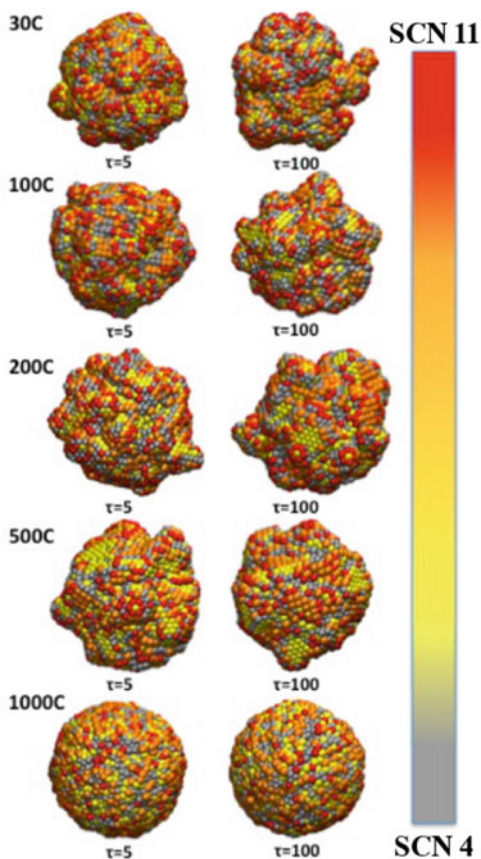
kinks with coordination numbers of 4, 5 and 6, where oxygen-oxygen bonds can be readily broken. For the H oxidation (HOR) and evolution (HER) reactions [21], the desorption/adsorption of hydrogen increases with atoms in surface facets (with SCN of 7, 8 or 9) (Fig. 6.3).

6.4.2.2 Catalytic Activity in Pt Nanoparticles

Beyond the availability of different types of active sites, the time evolution of these sites determines when the catalyst achieves maximum activity and can provide guidance as to when to stop growing. For instance, particles formed at $\tau = 2.5 \times 10^{-5}$ atoms per ns reach their maxima in only 0.5 ns, whereas the particles formed at higher rates at $\tau = 5 \times 10^{-4}$ atoms per ns, require 5 ns to reach maximal performance (see Fig. 6.4). This is not a simple relationship that can be predicted based on the rates alone, since the time evolution of the surface defects depends on the atomic diffusion rate which increases at lower depositions. Looking to the different classes of defects, we can see that surface facets and
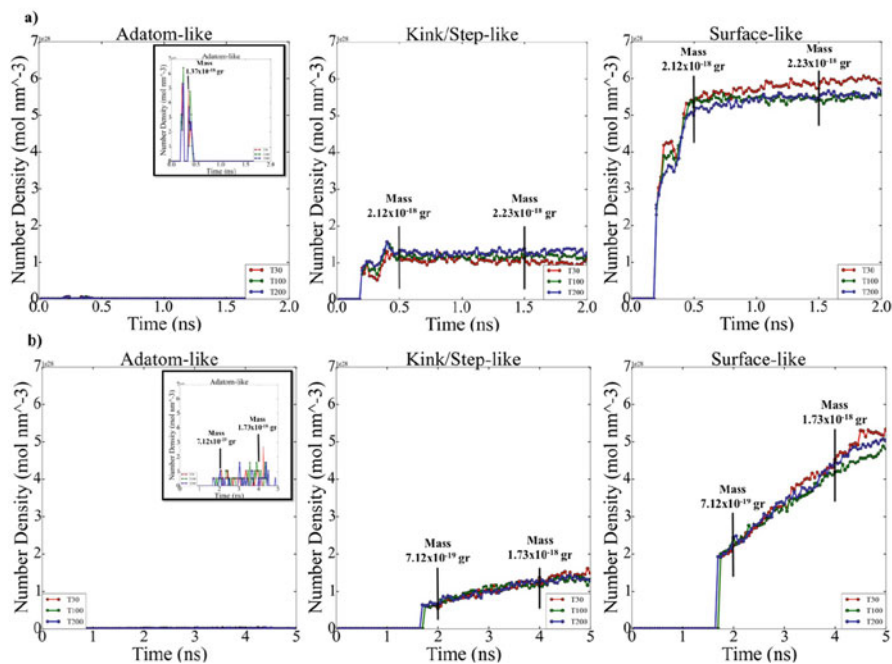
Fig. 6.4 Surface defects evolution. (**a**) Surface defects for Pt nanoparticles formed at atomic deposition rates of $\tau = 2.5 \times 10^{-5}$ atoms/ns. Adatom-like defects are present in the first 0.5 ns in the simulation in low amounts and then vanish as the nucleation continues. Kinks/steps-like defects achieved their maxima after 0.5 ns keeping this value constant along the simulation. Surface-like defects exhibit a higher number density of atoms with this defect, achieved after 0.5 ns maintaining this value constant during the simulation. (**b**) Surface defects for Pt nanoparticles formed at atomic deposition rates of $\tau = 5 \times 10^{-4}$ atoms/ns. Adatom-like defects are formed after 1.5 ns. Kinks/steps-like defects started to appear after 1.5 ns increasing the number density of atoms with this defect linearly until the end of the simulation. Surface-like defects are formed at 1.5 ns increasing the amount of atom linearly during the simulation and reaching the maxima at the end of the simulation. In all the simulations the temperature does not affect the evolution of the surface defects. The cluster size has been traced during nucleation in terms of their mass (This image is reproduced from reference [18])

surface microstructure dominate, indicating that these conditions produce particles more suitable for CO first-step reactions to break oxygen-oxygen bonds, HOR and HER reactions after the first 0.5 ns of the growth process in particles formed at $\tau = 2.5 \times 10^{-5}$ atoms per ns, which will be smaller, and at the end for particles formed at $\tau = 5 \times 10^{-4}$ atoms per ns, which will be larger (and therefore more expensive). The dependence of the SCN on the temperature does not contribute to the relative abundance of under-coordinated surface atoms; temperature curves exhibit similar values for the density of active sites in all the simulations; it is the atomic deposition rate that determines the surface. This is a useful finding, as the temperature can be selected to control the decomposition rate of the precursor without changing the relative abundance of under-coordinated active surface atoms.

6.5 Conclusions

In this chapter we have described some recent applications of various computational methods to understanding some basic principles of complex catalytic and electro-catalytic processes. These methods rely on either quantum-mechanical or statistical-mechanical principles, and the level of detail and the kind of insight into a certain catalytic problem depend on the system under investigation. Quantum-chemical electronic structure calculations, in practice usually DFT calculations, allow one to calculate binding energies and activation barriers of processes taking place on the catalyst surface. From many detailed calculations, it can be concluded that many adsorption processes and surface reactions are governed by the energy level of the d-band at the site where the process is taking place. We have illustrated how DFT calculations are useful to investigate electrochemical reactions on different surfaces. The model suggested by Norskov explains the H_2/CO electro-oxidation on Pt and Pt alloy surfaces. The DFT calculations also show that, unfortunately, the current models are too simplified to treat real catalysis effectively. Kinetic Monte Carlo is very useful in assessing the overall reactivity of a catalytic surface, which must include the effects of lateral interactions between adsorbates and the mobility of adsorbates on the surface in reaching the active sites. The importance of treating lateral interactions was demonstrated in detailed *ab initio*-based dynamic Monte Carlo simulations of ethylene hydrogenation on palladium and PdAu alloys. Surface diffusion of CO on alloy surfaces was shown to be essential to explain the qualitative features of the experimental CO stripping. The combination of first-principles approximation with KMC in ethylene hydrogenation has been proven to be very efficient to describe catalytic activity. Future models should consider this hybrid approximation as a starting point to improve the description of catalytic activity. Finally, CMD simulations were carried out to investigate the nucleation, growth and catalytic activity of Pt nanoparticles by analysing the surface atom coordination and final shapes. The formation of these nanoparticles under different temperature and deposition conditions shows that the atomic deposition rates lead to the coalescence and sintering conditions that act as an activation for the reorganisation of the atomic surface structure and distribution of active sites. In this context, nanoparticles formed at slower atomic deposition rates have the tendency to exhibit inhomogeneous surfaces with a higher density of under-coordinated atoms. This directly impacts the catalytic activity for many technologically important reactions. The particles obtained in the conditions considered herein are more suited to CO oxidation HER and HOR reactions. This method is a more "realistic" way to produce nanoparticles compared with other computational studies in which the particles are highly symmetric no considering surface defects as experimental evidence reveal.

References

1. M.P. Allen, D.J. Tildesley, *Computer Simulation of Liquids* (Oxford University Press, Oxford, 1987)
2. D.P. Landau, K. Binder, *A guide to Monte Carlo Simulations in Statistical Physics* (Cambridge University Press, Cambridge, 2000)
3. B.J. Berne, D. Thirumalai, Ann. Rev. Phys. Chem. **37**, 401 (1986)
4. K.E. Schmidt, D. Ceperley, *Monte Carlo Techniques for Quantum Fluids, Solids and Droplets* (Springer, Berlin, 1992)
5. C.J.H. Jacobsen, S. Dahl, B.S. Clausen, S. Bahn, A. Logadottir, J.K. Nørskov, J. Am. Chem. Soc. **123**, 8404 (2001)
6. J. Greeley, T.F. Jaramillo, J. Bonde, I.B. Chorkendorff, J.K. Norskov, Nat. Mater. **5**, 909 (2006)
7. J. Greeley, M. Mavrikakis, Nat. Mater. **3**, 810 (2004)
8. D.A. Hansgen, D.G. Vlachos, J.G.G. Chen, Nat. Chem. **2**, 484 (2010)
9. H. Toulhoat, P. Raybaud, J. Catal. **216**, 63–72 (2003)
10. P. Strasser, Q. Fan, M. Devenney, W.H. Weinberg, P. Liu, J.K. Norskov, J. Phys. Chem. B **107**, 11013 (2003)
11. F. Besenbacher, I. Chorkendorff, B.S. Clausen, B. Hammer, A.M. Molenbroek, J.K. Norskov, I. Stensgaard, Science **279**, 1913 (1998)
12. J.K. Norskov, T. Bligaard, J. Rossmeisl, C.H. Christensen, Nat. Chem. **1**, 37 (2009)
13. T. Bligaard, J.K. Norskov, S. Dahl, J. Matthiesen, C.H. Christensen, J. Sehested, J. Catal. **224**, 206 (2004)
14. M. Neurock, E.W. Hansen, Comput. Chem. Eng. **22**, S1045 (1998)
15. K. Reuter, D. Frenkel, M. Scheffler, Phys. Rev. Lett. **93**, 1 (2004)
16. L. Yang, P. Liu, Top. Catal. **57**, 125 (2014)
17. D. Mei, R. Rousseau, S.M. Kathmann, V.A. Glezakou, M.H. Engelhard, W. Jiang, C. Wang, M.A. Gerber, J.F. White, D.J. Stevens, J. Catal. **271**, 325 (2010)
18. H. Barron, G. Opletal, R. Tilley, A.S. Barnard, Catal. Sci. Technol. **6**, 144 (2015)
19. N. Tian, Z.Y. Zhou, S.G. Sun, J. Phys. Chem. C **112**, 19801 (2008)
20. J.S. Spendelow, Q. Xu, J.D. Goodpaster, P.J.A. Kenis, A. Wieckowski, J. Electrochem. Soc. **154**, F238 (2007)
21. Q.S. Chen, F.J. Vidal-Iglesias, J. Solla-Gullón, S.G. Sun, J.M. Feliu, Chem. Sci. **3**, 136 (2012)
22. P. Hohenberg, W. Kohn, Phys. Rev. Lett. **136**, B864 (1964)
23. W. Kohn, L. Sham, J. Phys. Rev. Lett. **140**, A1133 (1965)
24. J. Rossmeisl, E. Skulason, M.E. Bjorketun, V. Tripkovic, J.K. Norskov, Chem. Phys. Lett. **466**, 68–71 (2008)
25. R. Iftimie, P. Minary, M.E. Tuckerman, PNAS **102**, 6654–6659 (2005)
26. C.D. Taylor, S.A. Wasileski, J.N.M. Filhol, Phys. Rev. B **73**, 165402 (2006)
27. J. Filhol, M. Neurock, Angew. Chem. Int. Ed. **45**, 402–406 (2006)
28. J. Rossmeisl, J.K. Norskov, C.D. Taylor, M.J. Janik, M. Neurock, J. Phys. Chem. B **110**, 21833–21839 (2006)
29. M.J. Janik, C.D. Taylor, M. Neurock, J. Electroanal. Chem. Soc. **156**, B126–B135 (2009)
30. J.K. Norskov, J. Rossmeisl, A. Logadottir, L. Lindqvist, J. Kitchin, T. Bligaard, J. Phys. Chem. B **108**, 17886–17892 (2004)
31. P. Liu, A. Logadottir, J.K. Norskov, Electrochim. Acta **48**, 3731–3742 (2003)
32. J.K. Norskov, T. Bligaard, A. Logadottir, J. Kitchin, J.G. Chen, J. Electrochem. Soc. **152**, J23–J26 (2005)
33. A. Kowal, M. Li, M. Shao, K. Sasaki, M.B. Vukmirovic, J. Zhang, Nat. Mater. **8**, 325–330 (2009)
34. D.B. Ingram, S. Linic, J. Electrochem. Soc. **156**, B1457–B1465 (2009)
35. K. Sasaki, H.C.Y. Naohara, Y.M. Choi, P. Liu, M.B. Vukmirovic, Angew. Chem. Int. Ed. **49**, 8602–8607 (2010)

36. J.X. Wang, H. Inada, L. Wu, Y. Zhu, Y. Choi, P. Liu, J. Am. Chem. Soc. **131**, 17298–17302 (2009)
37. D.T. Gillespies, J. Comp. Phys. **22**, 403 (1976)
38. R.M. Nieminen, A.P. Jansen, J. Appl. Catal. A **160**, 99 (1997)
39. J.J. Lukkien, J.P.L. Segers, P.A.J. Hilbers, R.J. Gelten, A.P. Jensen, J. Phys. Rev. **E58**, 2598 (1998)
40. M.T.M. Koper, A.P.J. Jansen, R.A. van Santen, J.J. Lukkien, P.A.J. Hilbers, J. Chem. Phys. **109**, 6051 (1998)
41. R.M. Ziff, E. Gulari, Y. Barshad, Phys. Rev. Lett. **56**, 2553 (1986)
42. G. Ertl, Angew. Chem., Int. Ed. **47**, 3524 (2008)
43. K. Reuter, M. Scheffler, Phys. Rev. B **73**, 045433 (2006)
44. B. Temel, H. Meskine, K. Reuter, M. Scheffler, H. Metiu, J. Chem. Phys. **126**, 204711 (2007)
45. M. Rieger, J. Rogal, K. Reuter, Phys. Rev. Lett. **100**, 016105 (2008)
46. H. Meskine, S. Matera, M. Scheffler, K. Reuter, H. Metiu, Surf. Sci. **603**, 1724 (2009)
47. M. Nagasaka, H. Kondoh, I. Nakai, T. Ohta, J. Chem. Phys. **126**, 044704 (2007)
48. J. Rogal, K. Reuter, M. Scheffler, Phys. Rev. B **77**, 155410 (2008)
49. D.J. Liu, J.W. Evans, Surf. Sci. **603**, 1706 (2009)
50. S. Volkening, J. Wintterlin, J. Chem. Phys. **114**, 6382 (2001)
51. M. Stamatakis, M. Christiansen, D.G. Vlachos, G. Mpourmpakis, Nano Lett. **12**, 3621 (2012)
52. J. Cortes, E. Valencia, Phys. Rev. E **71**, 046136 (2005)
53. J. Cortes, E. Valencia, J. Phys. Chem. B **110**, 7887 (2006)
54. J. Cortes, E. Valencia, Bull. Chem. Soc. Jpn. **81**, 1267 (2008)
55. L. Olsson, V.P. Zhdanov, B. Kasemo, Surf. Sci. **529**, 338 (2003)
56. M. Rafti, J.L. Vicente, Phys. Rev. E **75**, 061121 (2007)
57. S.J. Alas, L. Vicente, Surf. Sci. **604**, 957 (2010)
58. L. Alvarez-Falcon, L. Vicente, Int. J. Quantum Chem. **112**, 1803 (2012)
59. T. Fink, J.P. Dath, R. Imbihl, G. Ertl, J. Chem. Phys. **95**, 2109 (1991)
60. M.F.H. Vantol, J. Siera, P.D. Cobden, B.E. Nieuwenhuys, Surf. Sci. **274**, 63 (1992)
61. S.J. Alas, F. Rojas, I. Kornhauser, G. Zgrablich, J. Mol. Catal. A Chem. **244**, 183 (2006)
62. S.J. Alas, G. Zgrablich, J. Phys. Chem. B **110**, 9499 (2006)
63. M. Tammaro, J.W. Evans, J. Chem. Phys. **108**, 7795 (1998)
64. V.P. Zhdanov, J. Chem. Phys. **110**, 8748 (1999)
65. V.P. Zhdanov, Catal. Lett. **93**, 135 (2004)
66. O. Kortluke, V.N. Kuzovkov, W. von Niessen, Phys. Rev. Lett. **81**, 2164 (1998)
67. V.P. Zhdanov, Catal. Lett. **84**, 147 (2002)
68. D. Duca, L. Botar, T. Vidoczy, J. Catal. **162**, 260 (1996)
69. E.W. Hansen, M. Neurock, J. Catal. **196**, 241 (2000)
70. D.H. Mei, E.W. Hansen, M. Neurock, J. Phys. Chem. B **107**, 798 (2003)
71. M. Neurock, D.H. Mei, Top. Catal. **20**, 5 (2002)
72. F. Maillard, M. Eikerling, O.V. Cherstiouk, S. Schreier, E. Savinova, U. Stimming, Faraday Discuss. **125**, 357 (2004)
73. V.P. Zhdanov, B. Kasemo, Surf. Sci. **405**, 27 (1998)
74. V.P. Zhdanov, B. Kasemo, Phys. Rev. Lett. **81**, 2482 (1998)
75. E.V. Kovalyov, E.D. Resnyanskii, V.I. Elokhin, B.S. Bal'zhinimaev, A.V. Myshlyavtsev, Phys. Chem. Chem. Phys. **5**, 784 (2003)
76. R. Narayanan, M. El-Sayed, J. Phys. Chem. B **6**, 144–151 (2005)
77. C. Burda, X. Chen, R. Narayanan, M. El-Sayed, Chem. Rev. **105**, 1025–102 2005
78. M. Crespo-Quesada, A. Yarulin, M. Jin, Y. Xia, L. Kiwi-Minsker, J. Am. Chem. Soc. **133** 12787–12794 (2011)
79. Y. Xiong, J.M. McLellan, Y. Yin, Y. Xia, Angew. Chem. Int. Ed. **46** 790–794 (2007)
80. W. Yang, R.G. Parr, Proc. Nat. Acad. Sci. U S A **82**, 6723–6726 (1985)
81. T. Baker, B. Xu, S.C. Jensen, C.M. Friend, E. Kaxiras, Catal. Sci. Tech. **1**, 1166 (2011)
82. H. Barron, A.S. Barnard, Catal. Sci. Tech. **5**, 2848–2855 (2015)
83. A.S. Barnard, L.Y. Chang, ACS Catal. **1**, 76–81 (2011)

84. F. Baletto, C. Mottet, R. Ferrando, Phys. Rev. B **66**, 155420 (2002)
85. F. Baletto, C. Mottet, R. Ferrando, Phys. Rev. Lett. **90**, 135504 (2003)
86. T.J. Toai, G. Rossi, R. Ferrando, Faraday Discuss. **138**, 49–58 (2008)
87. M.M. Mariscal, S.A. Dassie, P.M. Leiva, J. Chem. Phys. **123** 184505 (2005)
88. http://lammps.sandia.gov
89. S.M. Foiles, M.I. Baskes, M.S. Daw, J. Phys. Rev. B **33** 7983–7991 (1988)
90. J. Ren, R.D. Tilley, Small **3**, 508–1512 (2007)
91. F. Calvo, Elsevier Science (2013). ISBN:9780123946164
92. N. Tian, Z.Y. Zhou, S.G. Sun, J. Phys. Chem. C **112**, 19801–19817 (2008)
93. J.S. Spendelow, X. Qinqin, J.D. Goodpaster, P.J.A. Kenis, A. Wieckowski, J. Electrochem. Soc. **154**, F238 (2007)